International Immunopharmacology 162 (2025) 115156

Contents lists available at ScienceDirect

International Immunopharmacology

journal homepage: www.elsevier.com/locate/intimp

Curcumin analogue C66 ameliorates the pathology of Alzheimer's disease through suppression of JNK signaling pathway

Li Xiong [a,b,1], Qin Yu [a,1], Linjie Chen [a,1], Yu Deng [a], Qi Ai [a], Xiaoxia Xu [a], Ziyao Meng [a], Fan Chen [a], Xia Zhao [a,b,c,*], Jurui Wei [a,**], Houming Yu [a,**]

[a] The First People's Hospital of Lin'an District, Affiliated Lin'an People's Hospital, Hangzhou Medical College, Hangzhou, Zhejiang, 310014, China
[b] School of Pharmacy, Hangzhou Medical College, Hangzhou, Zhejiang 311399, China
[c] Department of Pharmacy and Institute of Inflammation, Zhejiang Provincial People's Hospital, Affiliated People's Hospital, Hangzhou Medical College, Hangzhou, Zhejiang 310014, China

ARTICLE INFO

Editor: Yi-Chao Zheng

Keywords:
C66
β-Amyloid 1–42 (Aβ)
Alzheimer's disease (AD)
Neuronal injury
Neuroinflammation
C-Jun N-terminal kinase (JNK) pathway

ABSTRACT

Oxidative stress and neuroinflammation are two key pathological features in the early stage of Alzheimer's disease (AD), and they promote each other to further drive the progression of AD. Therefore, the development of therapeutic agents with dual anti-inflammatory and antioxidant properties represents a promising strategy for AD treatment. C66, a synthetic derivative of curcumin, protected PC12 cells and primary neurons from oxidative damage caused by Aβ. In addition, C66 alleviated Aβ-induced excessive inflammatory response in BV2 cells. Further results showed that C66 reduced neuroinflammation and neuronal apoptosis, ultimately improved cognitive decline in APPswe/PSEN1dE9 (APP/PS1) double transgenic AD mice. Importantly, C66 exhibited superior improved properties in APP/PS1 mice compared with the clinical control drug donepezil. Mechanistically, we indicated that C66 conferred its neuroprotective effects by inhibiting c-Jun N-terminal kinase (JNK) pathway. The result was further confirmed by using SP600125, a specific JNK inhibitor. Together, our findings suggest that C66 is expected to be further developed as a drug candidate for AD therapy.

1. Introduction

Alzheimer's disease (AD) is the most common form of dementia, mostly affecting people over 65 years old. With the acceleration of the aging process, the number of AD patients will continuously escalate year on year, imposing an immense economic and emotional toll on both families and society [1]. Currently, only a limited number of Food and Drug Administration (FDA)-approved drugs are available for AD treatment, most of which demonstrate suboptimal efficacy and significant adverse effects [2]. This critical gap in therapeutic options has propelled the search for novel AD treatments to the forefront of biomedical research.

The pathogenesis of AD involves progressive neuronal damage, which constitutes a primary mechanism underlying the characteristic learning and memory impairments [3]. Accumulating evidence suggests that neuroprotection strategies can effectively ameliorate cognitive deficits. For example, dexmedetomidine prevented neuronal apoptosis in the hippocampus by regulating the miR-129-YAP1-JAG1 axis, thus improving cognitive impairment in mice with AD [4]; Astragalin reduced Aβ1–42-induced neuronal damage and ameliorated cognitive deficits in SAMP8 mice [5]; Red ginseng attenuated Aβ-induced mitochondrial damage and Aβ-mediated pathology in an animal model of AD [6]. Notably, neuronal damage and neuroinflammation engage in a vicious cycle that exacerbates AD progression. Damaged neurons release

Abbreviations: AD, Alzheimer's disease; Aβ, Amyloid-beta; APP/PS1, APPswe/PSEN1dE9; JNK, c-Jun N-terminal kinase; MAPK, Mitogen-activated protein kinase; CNS, Central nervous system; APP, Amyloid precursor protein; MTT, 3-(4,5-dimethylthiazol-2-yl)-2,5-Diphenyl tetrazolium bromide; LDH, Lactate dehydrogenase; ROS, Reactive oxygen species; JC-1, Mitochondrial membrane potential dye; PVDF, Polyvinylidene fluoride; WT, Wild-type; MWM, Morris water maze; NOR, Novel object recognition; RT-qPCR, Real time quantitative polymerase chain reaction; TNF-α, Tumor necrosis factor-α; IL-1β, Interleukin 1-beta; IL-6, Interleukin-6; IL-18, Interleukin-18; Map2, Microtubule-associated protein 2; PSD95, Postsynaptic density protein 95.

* Corresponding author at: School of Pharmaceutical Sciences, Hangzhou Medical College, Hangzhou, Zhejiang 311399, China.
** Corresponding authors.
E-mail addresses: xiazhao@hmc.edu.cn (X. Zhao), weiruirui03@126.com (J. Wei), yuhouming99@163.com (H. Yu).
[1] These author contribute equal.

https://doi.org/10.1016/j.intimp.2025.115156
Received 16 April 2025; Received in revised form 15 June 2025; Accepted 26 June 2025
Available online 3 July 2025

intracellular components that activate immune responses, thereby amplifying central nervous system inflammation [7]. Conversely, inflammatory mediators and reactive oxygen species generated during neuroinflammation further compromise neuronal integrity and promote apoptotic pathways. Given this reciprocal relationship, therapeutic agents capable of concurrently addressing both neuroprotection and anti-inflammatory mechanisms may demonstrate superior clinical efficacy compared to single-target approaches for AD management.

C66, a synthetic derivative of curcumin, has attracted significant interest due to its potent anti-inflammatory and anti-apoptotic properties, which demonstrate therapeutic potential across multiple disease models. For instance, C66 has been shown to counteract hyperglycemia-induced inflammation and cellular damage, as well as attenuate obesity-related myocardial injury [9]. However, its potential roles in treating AD remain unknown. Notably, C66 is currently being evaluated in clinical trials as a capsule formulation for diabetic nephropathy, underscoring its translational potential [10]. Given that diabetic patients exhibit a higher susceptibility to AD compared to non-diabetic individuals, this association raises an intriguing possibility: C66 may also hold therapeutic promise for AD. The shared pathological mechanisms between diabetes and AD including chronic inflammation, oxidative stress, and metabolic dysfunction urther support the rationale for investigating C66's potential neuroprotective effects in AD models.

c-Jun N-terminal kinase (JNK), a key member of the mitogen-activated protein kinase (MAPK) family, plays a central role in regulating critical physiological and pathological processes, including cell proliferation, apoptosis, oxidative stress, and inflammatory responses [11]. Emerging evidence highlights JNK as a promising therapeutic target in AD, where it mediates signaling pathways associated with neuronal apoptosis and neuroinflammation [12]. Under physiological conditions, JNK predominantly localizes to the cytoplasm. However, under pathological stress, JNK undergoes phosphorylation, triggering its nuclear translocation [5]. Once activated, phosphorylated JNK upregulates the transcription of pro-apoptotic factors while simultaneously modulating mitochondrial function. This includes downregulating the anti-apoptotic protein Bcl-2, upregulating the pro-apoptotic protein Bax, and ultimately activating Caspase-3, culminating in neuronal apoptosis [13]. In microglia, JNK activation further exacerbates neuroinflammation. Phosphorylated JNK promotes P65 phosphorylation, facilitating its nuclear translocation and subsequent transcription of pro-inflammatory cytokines such as TNF-α and IL-6 [14]. Given its dual role in promoting neuronal death and neuroinflammation, pharmacological inhibition of the JNK pathway represents a promising strategy for AD therapy. Notably, C66 has demonstrated therapeutic efficacy in various disease models by suppressing JNK signaling [15]. However, whether C66 exerts neuroprotective effects in AD via JNK inhibition remains to be experimentally validated.

In the present study, we evaluated the potential of C66 in AD therapy through both *in vivo* and *in vitro* experiments. SP600125, a selective inhibitor of JNK, was used to validate the action mechanism of C66. Our findings demonstrated for the first time that inhibition of JNK by C66 exhibited promise in the treatment of AD, and the improved properties of C66 were superior to the current clinical control drug donepezil (DON).

2. Materials and methods

2.1. Reagents

C66 (purity: HPLC ≥ 98 %) was obtained from Wenzhou Medical University (Wenzhou, China). Dimethyl sulfoxide (DMSO, D2650), Dulbecco's modified eagle's medium (DMEM, D6429), and bovine serum albumin (BSA, V900933) were purchased from Sigma (St. Louis, MO, USA). The phosphatase inhibitor and protease inhibitor cocktail (78440) were procured from Thermo Fisher Scientific (Rockford, IL, USA). The Annexin V-FITC/PI apoptosis detection kit (556547) was purchased from BD Biosciences (San Diego, CA, USA). Fetal bovine serum (FBS, 10099141C), Penicillin/streptomycin and neurobasal medium (10888022) were obtained from Gibco (Carlsbad, CA). PVDF membranes (1620177) were purchased from Bio-Rad (Shanghai, China). MTT powder (ST316), JC-1 staining assay (C2005), DAPI dye (C1006), DCFH-DA reagent (S0034S), Tunel assay (C1088), SP600125 (S1876-25 mg), and RIPA lysis buffer (P0013B) were bought from the Beyotime Institute of Biotechnology (Shanghai, China). β-Amyloid-1-42 (Aβ), NH2-DAEFRHDSGYEVHHQKLVFFAEDVGSNKGAIIGLMVGGV-VIA—COOH ($C_{203}H_{311}N_{55}O_{60}S$; PA4391; Molecular mass: 4514.10), was bought from Ontores biotechnology (Zhejiang, China). The antibodies and primers used in this study are presented in Table 1.

2.2. Cell culture and treatments

PC12 cells, a rat pheochromocytoma-derived cell line with neuronal characteristics, and BV2 cells, a well-established model for neuroinflammation studies, were maintained under standard culture conditions [16]. Both cell lines were cultured in 75 cm^2 flasks containing DMEM supplemented with 10 % fetal bovine serum (FBS) and 0.1 % penicillin-streptomycin (*v/v*), and incubated at 37 °C in a humidified 5 % CO_2 atmosphere. Culture media were replaced every 24–48 h to maintain optimal growth conditions. For cell subculture, cells were harvested at 80–90 % confluency using 0.25 % trypsin digestion, followed by centrifugation at 1000 rpm for 5 min. The cell pellet was then resuspended in fresh complete DMEM medium for subsequent passages.

2.3. Aβ oligomer preparation

Aggregation of amyloid-β (Aβ) protein represents a critical pathogenic event in AD, contributing to plaque formation, synaptic dysfunction, neuroinflammation, and ultimately cognitive decline [17]. Among various Aβ isoforms, Aβ1–42 demonstrates particularly high aggregation propensity and neurotoxicity. Aβ oligomers have been shown to exert potent neurotoxic effects, including neuronal apoptosis, glial activation, and memory impairment [18]. Based on these considerations, we employed Aβ1–42 oligomers as our in vitro AD model. The oligomers were prepared by initially dissolving Aβ1–42 in sterile DMSO to create a 10 mM stock solution. Following established protocols, we induced oligomer formation through 7-day incubation at 37 °C. For experimental use, the pre-aggregated Aβ1–42 solution was further diluted to a working concentration of 20 μM using culture medium.

2.4. MTT assay

The MTT reagent was prepared by dissolving 0.5 g of MTT powder in 100 mL of 1 × PBS to achieve a stock concentration of 5 mg/mL. The solution was thoroughly mixed until complete dissolution, then sterile-filtered through a 0.22-μm membrane. Aliquots were protected from light and stored at −20 °C until use. Cells were cultured in a complete medium with a seeding density of 7×10^3 cells/well in a 96-well plate. Following the required treatments, removed the medium from the cell culture wells and added the MTT solution, 20 μL/well. Incubated the cells at 37 °C for 4 h. After the incubation, carefully removed the MTT solution and added 100 μL of DMSO to each well in order to dissolve the formazan crystals formed by the viable cells. Finally, gently agitated the plates and measured the absorbance of the solubilized formazan solution at a wavelength of 570 nm with a microplate reader (SpectraMax 250, Molecular Devices, Sunnyvale, CA, USA).

2.5. Measurement of mitochondrial membrane potential (△ψm)

Mitochondrial membrane potential (Δψm) was evaluated using the JC-1 fluorescent probe (Beyotime Biotechnology, Cat# C2006, China) following the manufacturer's instructions. Briefly, after appropriate treatments, cells were incubated with the prepared JC-1 working

Table 1
Antibody and primer information.

Antibodies			
Antibody	Cat. NO	Source	Dilution
PSD95	2507	CST[a]	WB[b]:1:1000
MAP2	4542	CST	WB:1:1000
Iba1	17198	CST	IF[c]:1:200
GFAP	3670	CST	IF:1:200
APP/β-Amyloid	2450	CST	WB:1:1000/IF:1:200
P65	8242	CST	WB:1:500
p-P65	3033	CST	WB:1:500
JNK	9252	CST	WB:1:1000
p-JNK(Thr183/185)	4668	CST	WB:1:1000
TNF-α	3707	CST	WB:1:1000
IL-1β	12242	CST	WB:1:1000
IL-18	57058	CST	WB:1:1000
Bax	2774	CST	WB:1:1000
Bcl-2	15071	CST	WB:1:1000
NeuN	24307	CST	IF:1:200
cleaved-Caspase3	9661	CST	WB:1:1000
GAPDH	AF0006	Beyotime	WB:1:2000
Anti-rabbit IgG HRP	A0208	Beyotime	WB:1:2000
Anti-mouse IgG HRP	A0216	Beyotime	WB:1:2000
Alexa Fluor® 594	8889	CST	IF:1:500
Alexa Fluor® 488	4412	CST	IF:1:500
Primer			
Gene	**Species**	**Forward Primer (5′-3′)**	**Reverse Primer (5′-3′)**
TNF-α	Mouse	GAATGCTGGTGTATAAGTCTG	TATGTCATCAACTCGGTCAA
IL-1β	Mouse	GCAGGCAGTATCACTCATT	CAGCAGGTTATCATCATCATC
IL-6	Mouse	CCTCTGGTCTTCTGGAGTA	ATGAATTGGATGGTCTTGGT
GAPDH	Mouse	ACCTGCCAAGTATGATGAC	CTGTTGCTGTAGCCGTATT

Abbreviations: [a]CST: Cell Signaling Technology; [b]WB: western blot; [c]IF: Immunofluorescence.

solution at 37 °C for 30 min, which was dissolved in FBS-free medium and at a recommended concentration of 10 μg/mL. Then, carefully removed the JC-1 working solution and washed the cells twice with 1 x PBS to remove any unbound dye. At last, added fresh medium to the cells and proceeded with further experimental analysis. Fluorescent images in red (excitation, 560 nm; emission, 595 nm) and green (excitation, 485 nm; emission, 535 nm) were captured using a fluorescence inverted microscope. The JC-1 red/green fluorescence intensity ratio was utilized for Δψm calculation, with all values being normalized to those of the Ctrl group.

2.6. Measurement of reactive oxygen species (ROS)

Intracellular reactive oxygen species (ROS) levels were detected using 2′,7′-dichlorodihydrofluorescein diacetate (DCFH-DA; Beyotime Biotechnology, Cat# S0033S) according to the manufacture protocol. Briefly, cells were incubated with 10 μM DCFH-DA (prepared in serum-free DMEM) for 1 h at 37 °C under light-protected conditions, followed by two washes with 1× PBS to remove unincorporated dye. Fluorescence imaging was immediately performed using an inverted fluorescence microscope (excitation: 488 nm; emission: 525 nm), with signal intensity proportional to intracellular ROS production.

2.7. Western blot

Protein extraction was performed using RIPA lysis buffer (strong formulation) supplemented with protease and phosphatase inhibitors (1:100 dilution), followed by quantification with a BCA protein assay kit (Thermo Fisher, #23225). After mixing with 5× loading buffer, samples were denatured at 95 °C for 10 min in a metal bath. Electrophoresis was conducted with 40 μg total protein per lane, followed by wet transfer (1.5 h at constant current) to methanol-activated 0.22-μm PVDF membranes. Membranes were blocked with 3 % BSA in TBST for 1 h at room temperature to prevent nonspecific binding, then incubated with primary antibodies (1:1000 dilution) overnight at 4 °C with gentle agitation. After three 6-min TBST washes, membranes were probed with HRP-conjugated secondary antibodies for 2 h at room temperature. Following additional washes, protein bands were visualized using chemiluminescent substrate (BCL reagent) and imaged with a Bio-Rad Gel Doc XR system (Hercules, CA, USA). Band intensity quantification was performed using ImageJ software (NIH, Bethesda, MD).

2.8. TUNEL staining

Cellular apoptosis was evaluated using TUNEL assay (Beyotime, Cat# C1090, Shanghai, China) according to the manufacturer's protocol. Briefly, treated cells were washed with 1× PBS and fixed with 4 % paraformaldehyde (PFA) for 30 min at room temperature. After PBS washing, cells were permeabilized with 0.1 % Triton X-100 for 10 min at 4 °C. The TUNEL reaction mixture was prepared by combining 5 μL terminal deoxynucleotidyl transferase (TdT) with 45 μL fluorescent labeling solution, then applied to samples and incubated in a humidified chamber at 37 °C for 1 h in the dark. Following three 1× PBS washes, apoptotic cells were visualized using fluorescence microscopy (excitation/emission: 488/530 nm) with positive staining indicating DNA fragmentation. Quantitative analysis was performed by counting TUNEL-positive cells in five random fields per sample.

2.9. Real time-qPCR (RT-qPCR)

BV2 cells were seeded in a 6-well plate and cultured for total RNA extraction using an RNA isolation kit. Total RNA was reverse-transcribed into complementary DNA (cDNA) using a reverse transcriptase kit according to the manufacturer's protocol. Quantitative PCR was performed using SYBR Premix Ex Taq II (TAKARA) on a Bio-Rad CFX96 Real-Time System (Bio-Rad, USA) with the following cycling conditions: initial denaturation at 95 °C for 30 s, followed by 40 cycles of 95 °C for 5 s and 60 °C for 30 s. Gene-specific primers (designed and synthesized by Youkang Biotechnology Co., Ltd., Zhejiang, China) were used at optimized concentrations (see Table 1 for sequences). Relative

gene expression was calculated using the $2^{-\Delta\Delta Ct}$ method, with GAPDH serving as the internal reference gene.

2.10. Primary neuron extraction and culture

Primary neurons were isolated from postnatal (within 24 h) C57BL/6 mice under aseptic conditions. Firstly, newborn C57 mice were sterilized with 75 % ethanol. Then, we washed mice with DMEM-HG 3 times and cut off their heads, peeling off their meninges and cutting heads into pieces. Subsequently, brain tissues were subjected to digestion in 0.125 % EDTA-trypsin (Gibco, USA) at 37 °C for 10 min. The digestion was then halted by adding 10 % FBS and centrifuging the samples at 110 g for 10 min. Following removal of the supernatant, the cells were suspended in DMEM/F12 medium supplemented with 10 % FBS and seeded onto poly-L-lysine-coated coverslips (0.1 mg/mL) from Sigma (USA) in 96-well plates for subsequent experiments. The cells were incubated at 37 °C in a humidified atmosphere consisting of 5 % CO2. After 4 h, the medium was replaced with serum-free Neurobasal medium containing 2 % B27 supplement and 1 % L-glutamine. Neurons were cultured for 14 days before the experiment, with half of the medium changed every day.

2.11. Animal treatment

APPswe/PSEN1dE9 (APP/PS1) double-transgenic mice (7-month-old females, ~30 g) were procured from the Jackson Laboratory and bred in Hangzhou Medical College animal facility. These mice were accommodated in laboratory condition that met the standard requirements for specific-pathogen-free (SPF) facilities. The experimental protocol was approved by the Hangzhou Medical College Animal Ethics Committee (2022−001). All mice were maintained at 24–26 °C, under a 12 h dark-light cycle, with food and water provided ad libitum. Animals were randomly divided into five groups ($n = 10$/group): wild-type (WT), APP/PS1, APP/PS1 + 1 mg/kg C66, APP/PS1 + 5 mg/kg C66 and APP/PS1 + 5 mg/kg donepezil (DON). C66 (1 mg/kg or 5 mg/kg, respectively) and DON were dissolved in 1 × PBS. C66 and DON were dissolved in 1 × PBS and administered daily by oral gavage for 6 weeks, with doses adjusted weekly based on body weight. Behavioral assessments, including novel object recognition (NOR) and Morris water maze (MWM) tests, were conducted following the treatment period.

2.12. Novel object recognition (NOR)

The NOR test was conducted in a 25 × 25 × 40 cm^3 arena to evaluate recognition memory in mice. After 24-h acclimatization to the testing environment, mice were individually placed in the arena containing two identical objects (Object A) for a 5-min familiarization trial, with exploration behavior (sniffing or touching within 2–3 cm) recorded via an overhead camera. Following a 24-h retention interval, one object was replaced with a novel object (Object B) and exploration times were recorded for another 5 min. Cognitive function was quantified using the discrimination index [(Time with novel object - Time with familiar object)/(Total exploration time)], where cognitively impaired mice typically show no preference, while normal mice demonstrate significant novel object preference [19]. All trials were conducted under consistent lighting conditions with objects and arena thoroughly cleaned between trials to eliminate odor cues.

2.13. Morris water maze (MWM)

Spatial learning and memory were assessed using the MWM test as previously described [20]. The apparatus consisted of a circular pool (100 cm diameter × 38 cm height) filled with water maintained at 22–26 °C, containing a hidden platform (6 cm diameter) positioned 1 cm below the water surface. Four distinct visual cues were equally spaced around the pool perimeter to provide spatial reference points. Mice were acclimated to the testing room 24 h prior to experimentation. The protocol included: (1) a 5-day acquisition phase with four daily trials (60 s/trial) to locate the hidden platform, and (2) a 60 s probe trial on day 6 with the platform removed to assess spatial memory retention. All sessions were conducted during consistent morning hours to minimize circadian influences. Movement trajectories and latency parameters were automatically recorded and analyzed using VisuTrack software (Xinxin Soft Information Technology Co., Shanghai, China).

2.14. Tissue sample preparation

Following humane euthanasia with chloral hydrate (0.25 mg/mL), mice underwent transcardial perfusion with ice-cold 1× PBS followed by 20 mL of 4 % paraformaldehyde (PFA) for tissue fixation. Brains were immediately extracted and divided for multiple processing protocols: one hemisphere was post-fixed in 4 % PFA for 24 h at 4 °C, cryoprotected in 30 % sucrose, embedded in optimal cutting temperature compound (OCT), and stored at −80 °C for cryosectioning; the contralateral hemisphere was dehydrated through graded ethanol series (75 %–100 %), paraffin-embedded using an EG1150 tissue processor (Leica), and stored at 4 °C for histological analysis; select brain regions were flash-frozen in liquid nitrogen and homogenized in RIPA lysis buffer for biochemical assays. All procedures were performed under RNase-free conditions when applicable.

2.15. Immunofluorescence (IF)

The OCT-embedded brain tissues were sectioned into 15-μm thick slices using a tissue slicer (Leica, CM1950). Tissue sections were permeabilized with 0.1 % Triton X-100 (Gibco) for 10 min and then incubated with a blocking buffer comprising 10 % BSA in 1 × PBS for 60 min at room temperature. Subsequently, the sections were subjected to incubation with primary antibodies at 4 °C overnight. The following day, the sections were washed three times with 1 × PBS and then exposed to the appropriate secondary antibodies (Alexa Fluor 488 anti-mouse or 594 anti-rabbit, 1:500) for 2 h at room temperature. Following this, all sections underwent three washes with 1 × PBS and were then mounted using a DAPI-containing anti-fluorescence quencher. Immunofluorescence images were captured using a Nikon A1 confocal microscope. Three independent experimental replicates were performed for each condition, with ≥3 tissue sections analyzed per replicate. Image quantification was performed using NIS-Elements AR software (Nikon) with thresholding maintained constant across all samples.

2.16. Enzyme-linked immunosorbent assay (ELISA)

Hippocampal tissues were homogenized in ice-cold 1× PBS supplemented with protease inhibitor cocktail (Pierce, Rockford, IL, USA) using a mechanical homogenizer. The homogenates were centrifuged at 12,000×*g* for 10 min at 4 °C to obtain clarified supernatants. Aβ1–40, Aβ1–42, and sAPPβ concentrations were quantified using commercial ELISA kits following the manufacturer's protocols. Absorbance was measured at 450 nm with wavelength correction at 570 nm using a SpectraMax microplate reader (Molecular Devices). All samples were run in duplicate, and analyte concentrations were calculated against standard curves generated for each plate. Data were normalized to protein content (determined by BCA assay) and expressed as percentage change relative to wild-type (WT) control values.

2.17. Statistical analysis

All data were analyzed using GraphPad Prism 8.0 (GraphPad Software, La Jolla, CA) and are presented as mean ± SEM from three independent experiments. For comparisons among multiple groups, one-way or two-way ANOVA was employed as appropriate, followed by Tukey's post hoc test for multiple comparisons. A probability value of $p < 0.05$ was considered statistically significant.

3. Results

3.1. C66 attenuates aβ-induced cytotoxicity in PC12 cells

The symmetrical aminocarbonyl curcumin derivative C66 (Fig. 1A) has demonstrated potent anti-apoptotic and anti-inflammatory properties in various disease models, prompting our investigation of its therapeutic potential for AD. At first, PC12 cells were seeded into 96-well plates and exposed to various concentrations of Aβ for 24 h. The MTT assay was used to assess cell viability, and 10 μM of Aβ was confirmed as the subsequent treatment concentration (Fig. 1B). Pretreatment with C66 for 30 min prior to Aβ exposure conferred significant neuroprotection in a concentration-dependent manner, with notable efficacy even at low doses and a wide therapeutic window (Fig. 1C). Given the pivotal role of oxidative stress in early apoptosis, we further characterized C66's protective effects using JC-1 mitochondrial membrane potential assays and DCFH-DA ROS detection. Quantitative analysis revealed that C66 pretreatment (1 μM) significantly attenuated Aβ-induced mitochondrial depolarization (Fig. 1D–E) and intracellular ROS accumulation (Fig. 1F–G). Western blot analysis of apoptotic markers demonstrated that C66 treatment normalized the Aβ-disrupted Bcl-2/Bax ratio (Fig. 1H–J). These findings collectively demonstrate that C66 effectively mitigates Aβ-induced neuronal damage through multiple protective mechanisms.

3.2. C66 inhibits aβ-induced inflammation in BV2 cells and is beneficial in protecting PC12 cells from damage

To investigate the anti-inflammatory effects of C66 in microglia, BV2 cells were pretreated with 5 μM C66 for 30 min prior to 10 μM Aβ exposure for 24 h. Quantitative PCR analysis revealed that Aβ stimulation significantly upregulated proinflammatory cytokine mRNA expression (*Tnfa, Il1b,* and *Il6*) compared to controls, while C66 pretreatment markedly suppressed these transcriptional responses (Fig. 2A). Further western blot results verified that compared with the Aβ group, the protein levels of TNF-α, IL-1β, and IL-18 were greatly decreased in the C66 + Aβ group (Fig. 2B).

It is well known that a large number of proinflammatory cytokines released by activated neuroimmune cells can cause damage to neurons [21]. Accordingly, the supernatant from cultured BV2 cells was added to

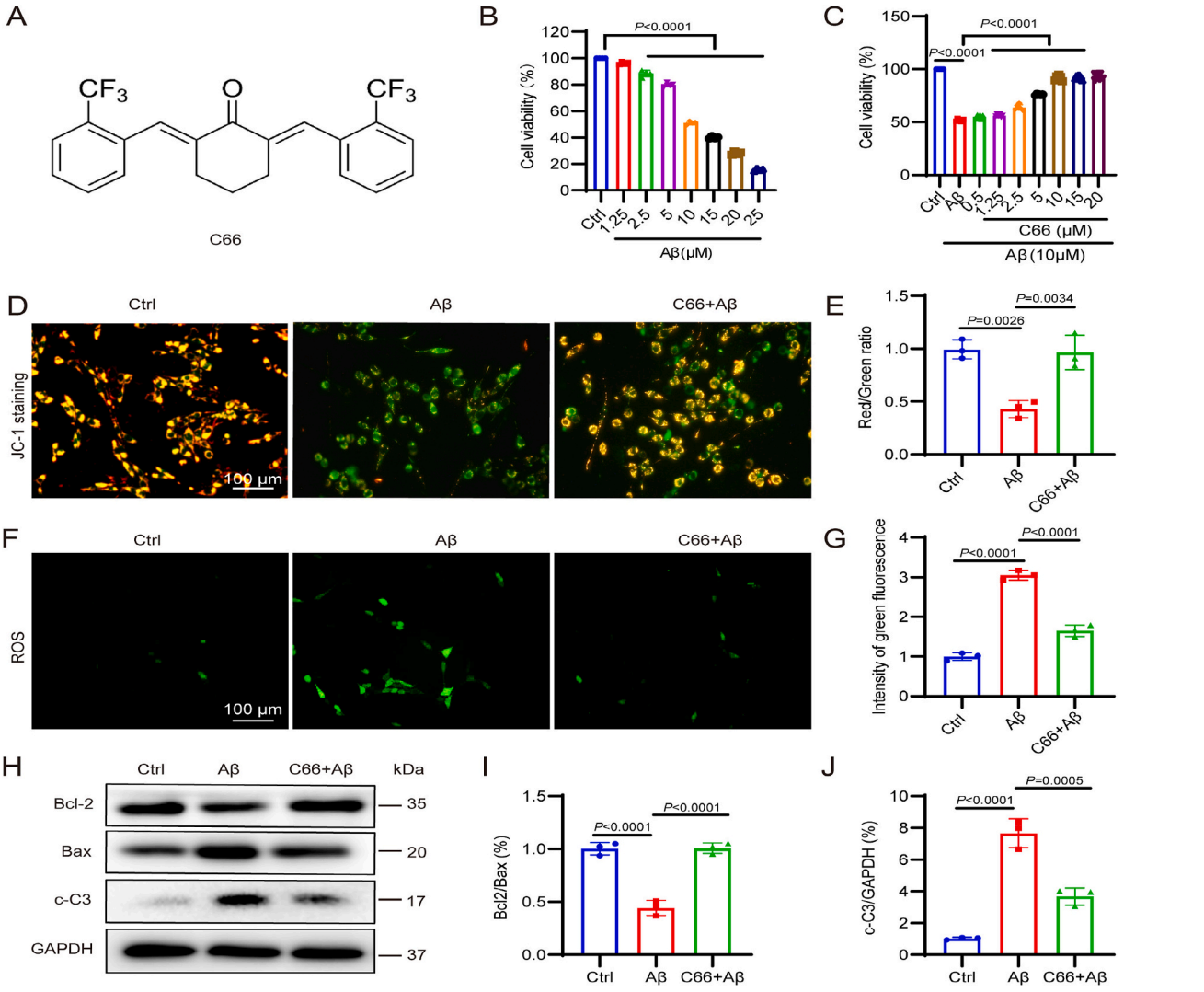

Fig. 1. C66 attenuates Aβ-induced PC12 cell injury. (A) The chemical structure of C66. (B) The effect of Aβ on PC12 cell viability was measured by an MTT assay. (C) PC12 cells were pretreated with various concentrations of C66 for 30 min, followed by 10 μM of Aβ for another 24 h. Cell viability was tested using MTT. (D) Representative images of JC-1 staining. (E) Ratio analysis of red/green fluorescence intensity in JC-1 staining by Image J software. (F) Representative images of ROS staining. (G) Quantification of green fluorescence intensity in ROS staining by Image J software. (H) Western blot analysis of Bcl-2, Bax and cleaved-Caspase3. GAPDH was used as a loading control. (I–J) Image J software quantification data of protein levels in I. (For interpretation of the references to colour in this figure legend, the reader is referred to the web version of this article.)

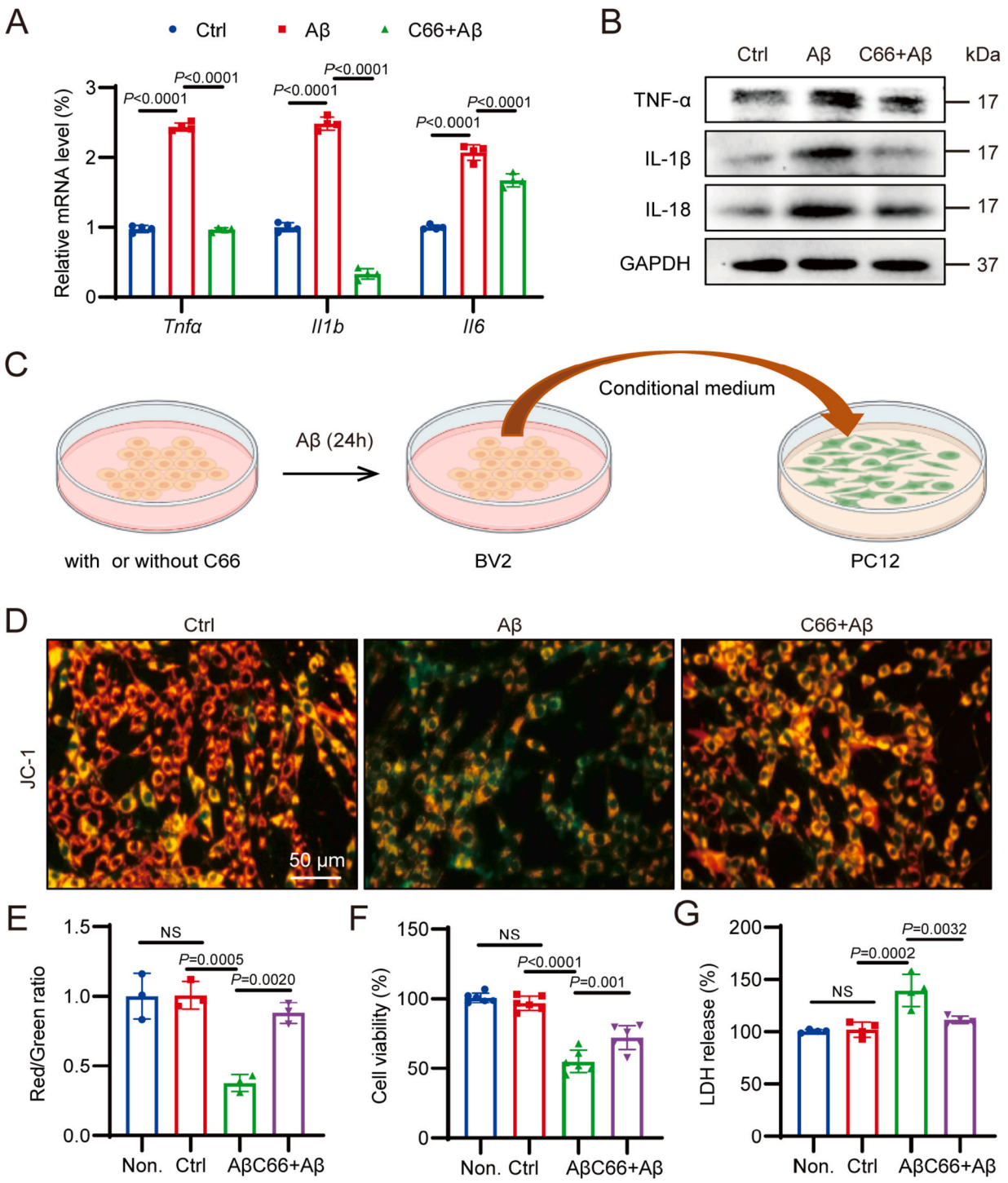

Fig. 2. C66 alleviates Aβ-induced inflammation in BV2 cells and mitigates PC12 cell damage resulting from inflammatory responses. (A) BV2 cells were pretreated with C66 at a concentration of 5 μM, followed by additional stimulation of 10 μM-Aβ for 24 h. RT-qPCR measurement of relative mRNA levels of *Tnfα*, *Il1b*, and *Il6*. (B) The expression levels of TNF-α, IL-1β, and IL-18 were examined by western blotting. (C) Process for collecting BV2 supernatants to treat PC12 cells. (D) BV2 cells were cultured and pretreated with or without 5 μM of C66 for 0.5 h, and then treated with 10 μM-Aβ for 24 h. The collected supernatants of BV2 were added to PC12 cells. Representative images of JC-1 staining in PC12. (E) Quantitative analysis of D. (F) Cell viability was measured by MTT in PC12. (G) The extent of membrane damage was determined using a LDH detection assay.

PC12 cells in the presence or absence of C66 (Fig. 2C). To detect mitochondrial membrane damage in PC12 cells, we performed JC-1 staining. Images showed compared to the Aβ group, the C66 + Aβ group had a higher red/green fluorescence intensity ratio (Fig. 2D–E). Then, we examined the viability of PC12 cells, and the result of MTT confirmed that 5 μM of C66 pretreatment effectively reduced harmful substances released by BV2 cells, thereby alleviating their damage to PC12 cells (Fig. 2F). What's more, the content of LDH release in the supernatant of the C66 + Aβ group was significantly lower compared to that of the Aβ group (Fig. 2G). These findings implied that pretreatment with C66 decreased the release of inflammatory factors in BV2 cells, which was beneficial to protect PC12 cells from injury.

3.3. C66 lessens aβ-induced PC12 damage by inhibiting JNK phosphorylation

To elucidate the mechanistic involvement of JNK signaling in C66-mediated neuroprotection, we first evaluated dose-dependent effects of C66 (30 min) on JNK phosphorylation in PC12 cells. Western blot analysis revealed significant suppression of JNK phosphorylation at 5 μM C66 (Fig. 3A–B). Subsequently, PC12 cells were pretreated with 1.25 μM of the specific JNK inhibitor SP600125 for 1 h, then treated with C66–10 μM for 0.5 h, and subsequently stimulated with 10 μM Aβ for 24 h. Western blot results indicated that there was no significant difference in the levels of p-JNK, Bcl-2/Bax, and cleaved Caspase3 between the C66 + Aβ group and the C66 + SP600125 + Aβ group (Fig. 3C–D). The conclusion was also comfirmed by the Tunel staining (Fig. 3E–F) and the MTT assay (Fig. 3G). In comparison to the Ctrl group, the Aβ group exhibited an increase in apoptosis rate and a decrease in cell viability; while the C66 + Aβ group and the C66 + SP600125 + Aβ group improved these adverse conditions, and no significant difference was observed between the two groups. The above results verified that C66 C66 exerts its neuroprotective effects primarily through JNK pathway suppression.

3.4. C66 alleviates aβ-induced inflammatory responses by inhibiting the JNK pathway in BV2 cells

It has been reported that C66 could alleviate inflammation by suppressing the JNK/P65 signaling pathway in SV40-MES-13 cells [8]. Therefore, we want to examine whether C66 also confers such a role in BV2 cells. In our study, BV2 cells were subjected to varying concentrations of C66 for a duration of 0.5 h to analyze the inhibitory efficiency of C66 on JNK phosphorylation, and we found that C66 significantly inhibited JNK phosphorylation at a concentration of 5 μM (Fig. 4A–B). Similarly, SP600125 was used to confirm the mechanism by which C66 functioned. Western blot results showed that there was no significant difference in the levels of p-JNK, p-P65, TNF-α, IL-1β, and IL-18 between the C66 + Aβ group and the C66 + SP600125 + Aβ group (Fig. 4C–D). Further, we performed immunofluorescence (IF) to detect the nuclear translocation of P65, which would further regulate the expression of

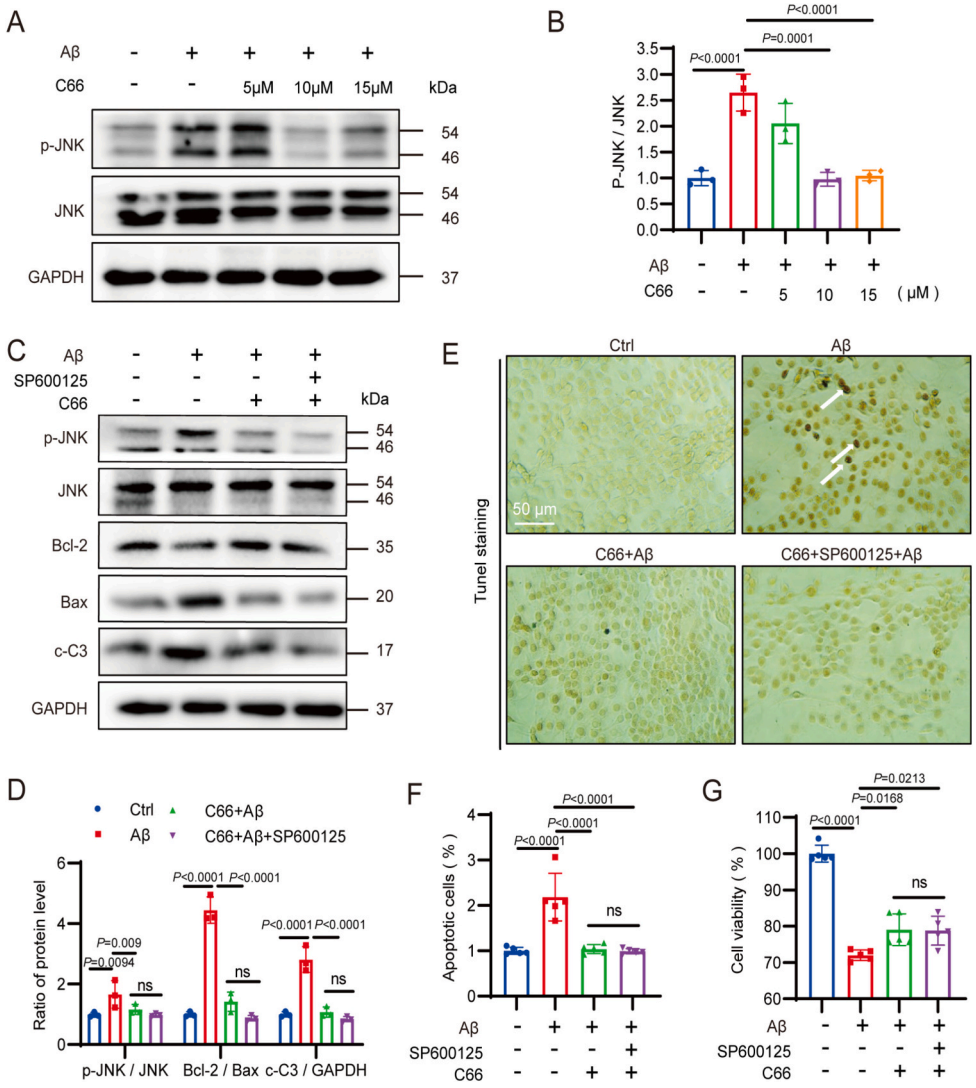

Fig. 3. C66 inhibit Aβ-induced JNK activation and reduced PC12 cell apoptosis by inhibiting the JNK pathway. (A) PC12 cells were treated with different concentrations of C66 for 30 min. WB was used to explore the inhibitory efficiency of C66 on JNK phosphorylation. (B) Quantification of the p-JNK/JNK protein level in A. (C) PC12 cells were pretreated with or without 1.25 μM of SP600125 (a specific inhibitor of JNK) for 1 h, followed by C66–10 μM treatment for 0.5 h and stimulation with 10-μM Aβ for another 24 h. Expression levels of p-JNK, JNK, Bcl-2, Bax, and cleaved-Caspase3 were detected by WB. (D) Quantitative analysis of A. All quantitative analysis results of WB bands were obtained by Image J software. (E–F) Representative images of tunel staining to detect cell apoptosis. (G) Cell viability was measured by the MTT assay.

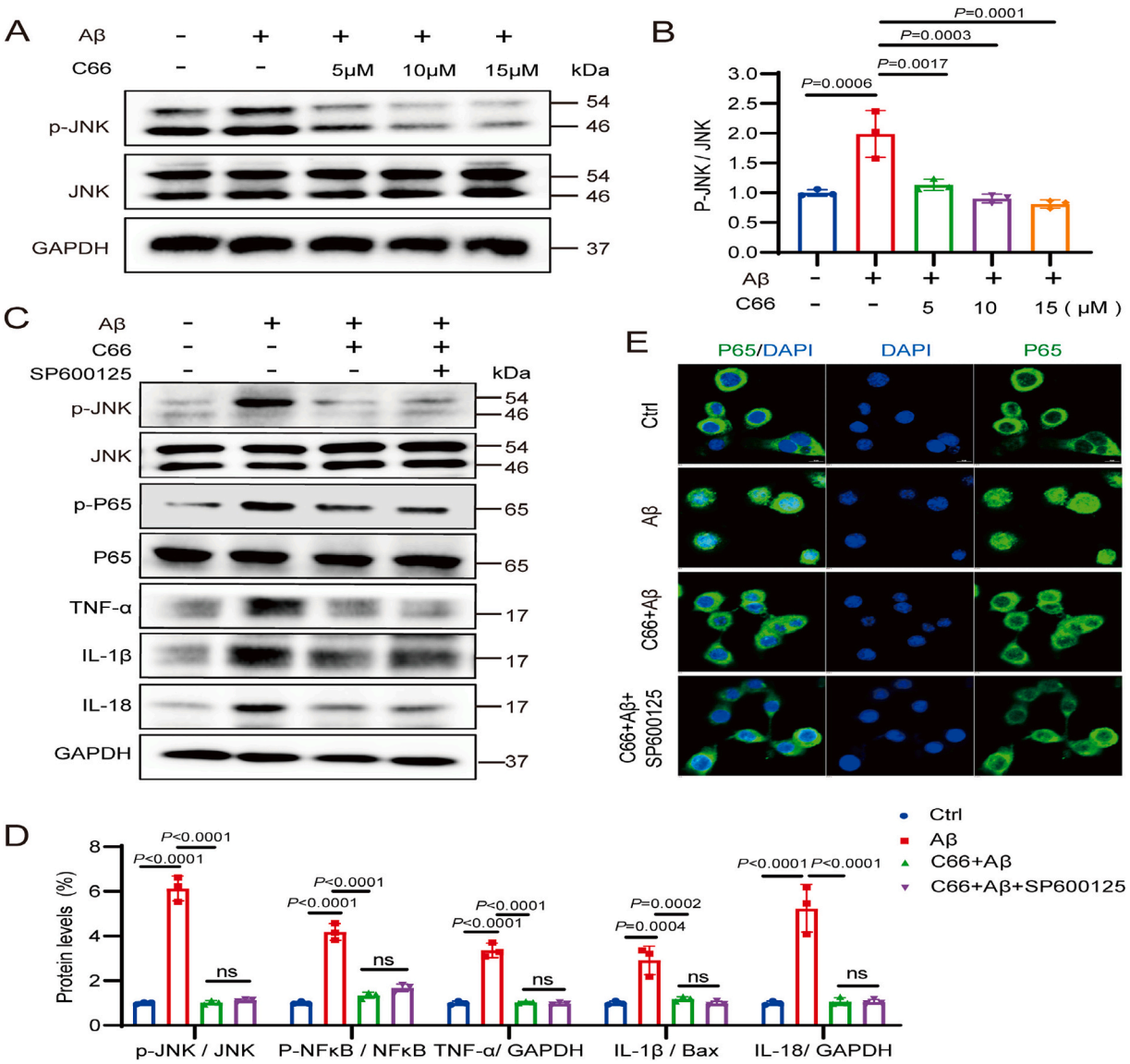

Fig. 4. C66 alleviates Aβ-induced inflammatory responses by inhibiting the JNK pathway in BV2 cells. (A) BV2 cells were treated with different concentrations of C66 for 30 min. WB was used to explore the inhibitory efficiency of C66 on JNK phosphorylation. (B) Quantification of the p-JNK/JNK protein level in A. (C–D) BV2 cells were pretreated with or without SP600125 at a concentration of 2.5 μM for 1 h, followed by 5-μM-C66 for 0.5 h and 10 μM-Aβ for 24 h. Western blot analysis of p-JNK, JNK, p-P65, P65, TNF-α, IL-1β and IL-18 in BV2 cells. (E) Representative images of P65 nuclear translocation.

genes related to inflammation. Confocal images showed more nuclear translocation of P65 in the Aβ group, compared to the Ctrl group; in contrast, this phenomenon was improved in both the C66 + Aβ group and the C66 + SP600125 + Aβ group without significant difference (Fig. 4E). Taken together, these data indicated that C66 alleviated Aβ-induced inflammation in BV2 possibly through the JNK signaling pathway.

3.5. C66 relieves aβ-induced cell damage in primary neurons

To further confirm the protective effect of C66 against Aβ-induced neurotoxicity, primary neurons were used for verification. Primary neurons were extracted from brains of newly born C57 mice (within 24 h) and identified by staining with the NeuN antibody (Fig. 5A). A portion of primary neurons were seeded in a 96-well plate and pretreated with C66–10 μM for 0.5 h. Then, 10 μM of Aβ was used to induce cell damage. As determined by the MTT experiment result, cell viability was higher in the C66 + Aβ group compared with the Aβ group (Fig. 5B). Images of JC-1 and ROS staining respectively indicated that C66 pretreatment could reverse the disturbance in mitochondrial membrane potential and decrease Aβ-induced ROS accumulation in primary neurons (Fig. 5C–F). In addition, a tunel staining assay was conducted to detect cell apoptosis, and we found that pretreatment with C66 alleviated Aβ-induced cell apoptosis (Fig. 5G–H). These findings in primary neurons corroborate our observations in PC12 cells. The concordance between transformed cell lines and primary neuronal cultures significantly strengthens the protective effect of C66 against Aβ-induced toxicity.

3.6. C66 ameliorates cognitive impairment in APP/PS1 mice

Thirty-week-old female APP/PS1 mice were randomly allocated to five treatment groups ($n = 10$/group): wild-type (WT) controls receiving 1× PBS, APP/PS1 controls receiving 1× PBS, APP/PS1 + 1 mg/kg C66, APP/PS1 + 5 mg/kg C66, and APP/PS1 + 5 mg/kg donepezil (DON). All treatments were administered daily via oral gavage for six weeks prior to behavioral assessment (Fig. 6A). Initially, we conducted the NOR test, and the representative mouse movement trajectory diagrams validated that C66 treatment increased the number of approaches and probe time

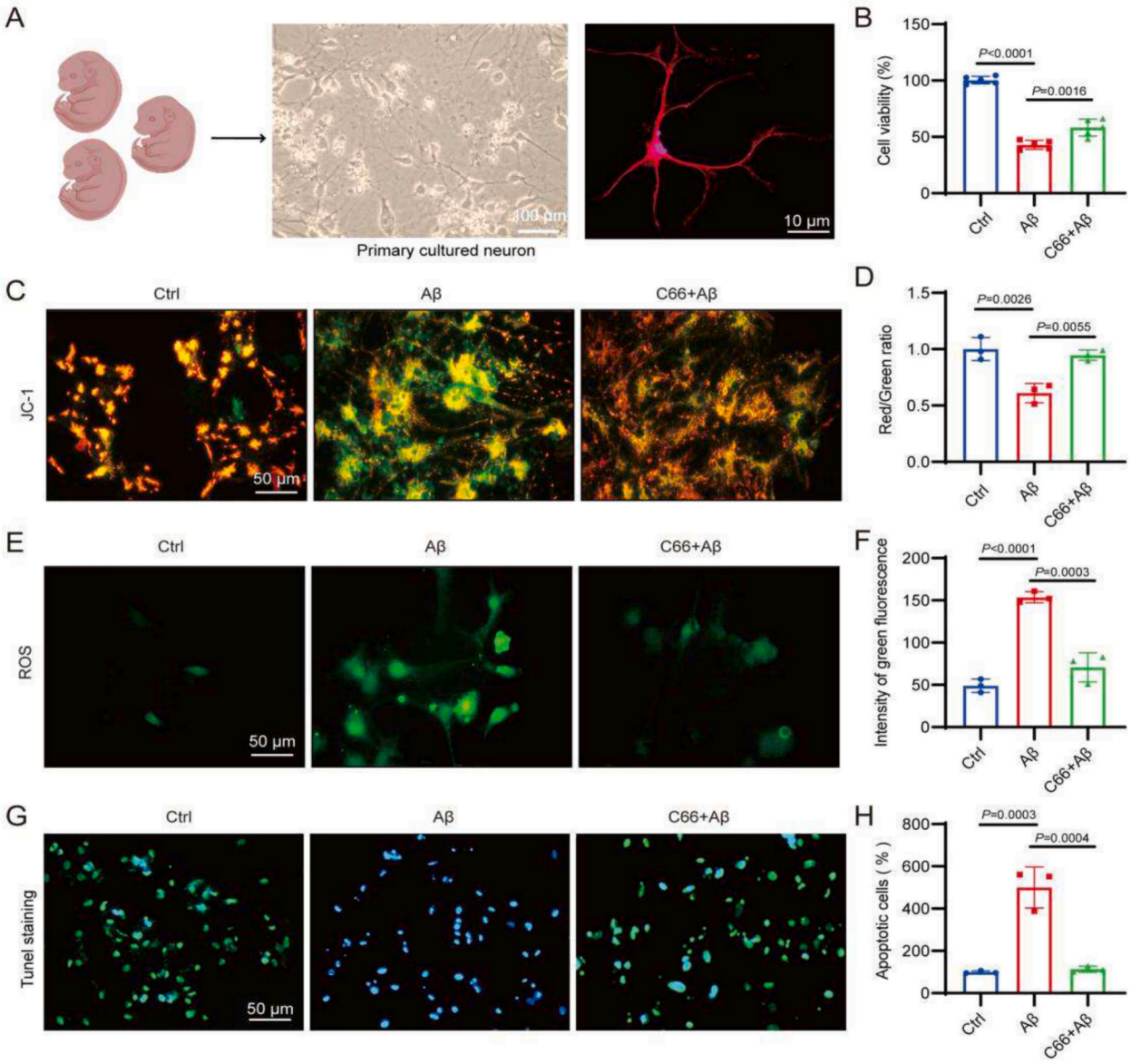

Fig. 5. C66 relieves Aβ-induced cell damage in primary neurons. Neural cells were extracted from brains of newborn C57 mice according to the procedure, and selected by specific medium to obtain the desired neuronal cells. (A) Images of primary neurons taken by a general microscope and a confocal microscope. (B) Primary neurons were pretreated with 10 μM of C66 for 0.5 h, then subject to stimulation of 10 μM-Aβ for 24 h. Cell viability was measured by an MTT assay. (C) Representative images of JC-1 staining. (D) Quantification of red/green fluorescence intensity in JC-1 staining. (E) Representative images of ROS staining. (F) Quantification of green fluorescence intensity in ROS staining. (G) Representative images of tunel staining in primary neurons. (H) Quantitative analysis of G. (For interpretation of the references to colour in this figure legend, the reader is referred to the web version of this article.)

for the new object on day 2 at a dose of 5 mg/kg, with an improved effect compared to the low-dose group (Fig. 6B–E). The subsequent MWM test results showed that APP/PS1 mice treated with C66 exhibited shorter escape latencies in the first 5 days compared with the APP/PS1 group. On day 6, APP/PS1 mice displayed a decrease in the number of platform crossings and a reduced amount of time spent in the target quadrant, while high-dose C66 or donepezil treatment greatly improved the aforementioned indicators and enhanced spatial learning and memory abilities of APP/PS1 mice. There was no intergroup differences in swimming speed and total distance among the mice in different groups , confirming that the effects were cognition-specific rather than motor-related. Importantly, C66 at a dose of 5 mg/kg provided an improvement effect superior to that of DON at 5 mg/kg (Fig. 6F–K). These comprehensive behavioral findings demonstrate that chronic C66 administration dose-dependently attenuates cognitive decline in APP/PS1 mice.

3.7. C66 ameliorates AD pathology of APP/PS1 mice

The multifaceted pathology of AD, characterized by amyloid plaque accumulation, synaptic dysfunction, neuronal degeneration, and neuroinflammatory responses [22,23], presents critical therapeutic targets. Compounds that can extensively alleviate these pathological features are expected to become AD treatment candidates. In our study, images of tissue immunofluorescence displayed that treatment with C66 or DON decreased the number of extracellular Aβ plaques in the hippocampus of APP/PS1 mice (Fig. 7A). Besides, using mouse hippocampal homogenates, we examined concentrations of different Aβ components and found that C66 or DON significantly decreased fragments cleaved by β-secretase, especially Aβ40 and Aβ42 (Fig. 7B–D). Further WB results obtained confirmed that C66 treatment reduced the level of APP/β-amyloid and significantly increased the levels of synapse-associated proteins, including PSD95 and MAP2, in the hippocampus of APP/PS1

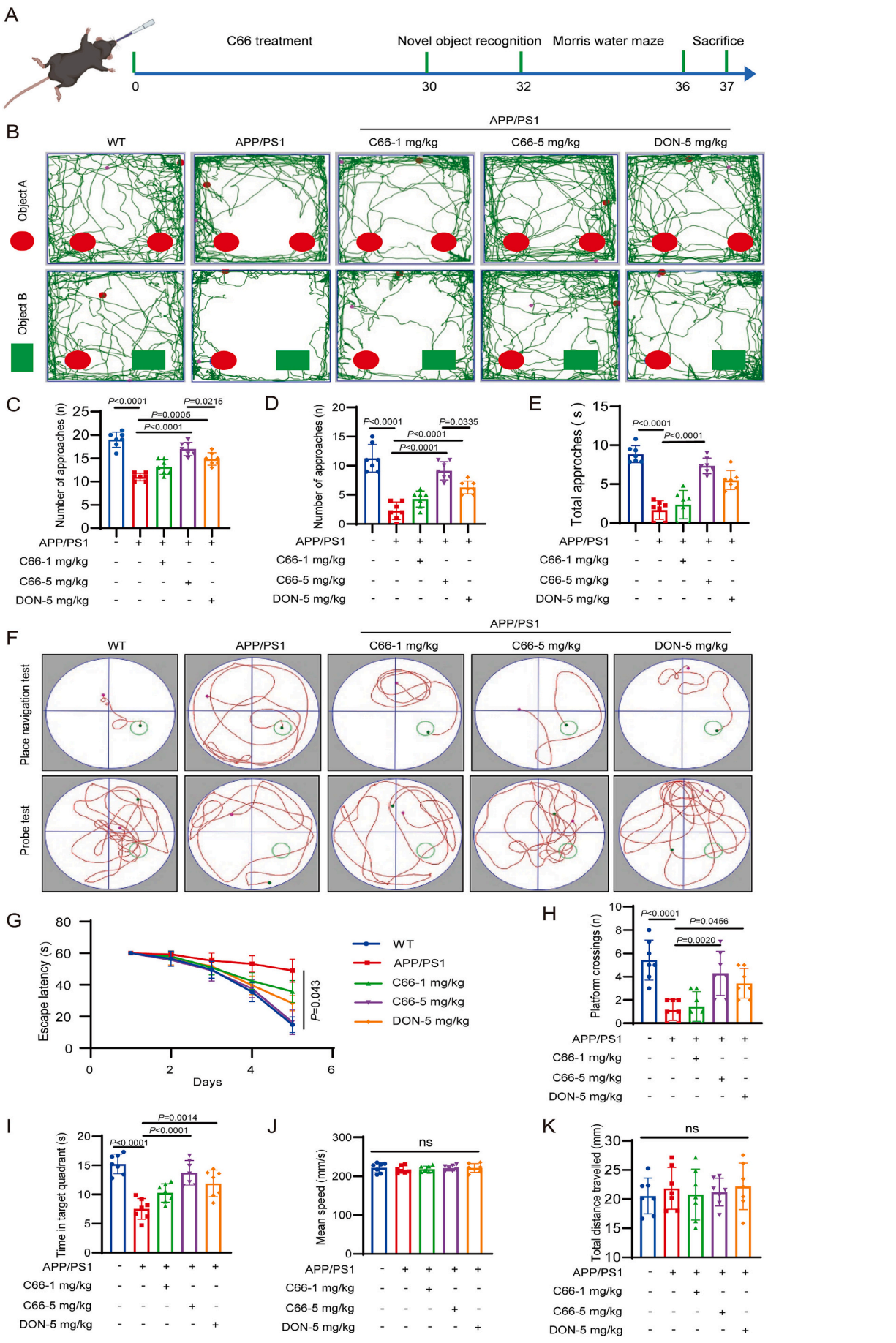

(caption on next page)

Fig. 6. C66 delays cognitive decline in APP/PS1 mice. 30-week-old female APP/PS1 mice were selected, and were intragastrically administered with C66 or DON once a day at a dose of 1 mg/kg or 5 mg/kg for 6 consecutive weeks. Mice from the WT or APP/PS1 group were given PBS solution in the same way. $n = 10$ mice per group. (A) Timeline of C66-treated APP/PS1 mice. (B) Representative images of the NOR test on day 1 and day 2. (C)The number of approaching to the object A on the second day. (D) The number of approaching to the new object B on the second day. (E) The probe time for the new object on day 2 of mice in each group. (F) Representative traces of the MWM test. (G) Escape latency on day 1–5. (H) Platform crossings of mice from different groups on day 6. (I) Time spent in the target quadrant where the platform was located on day 6. (J) The total swimming speed of each mouse within 60 s on day 6. (K) The total swimming distance of each mouse within 60 s on day 6.

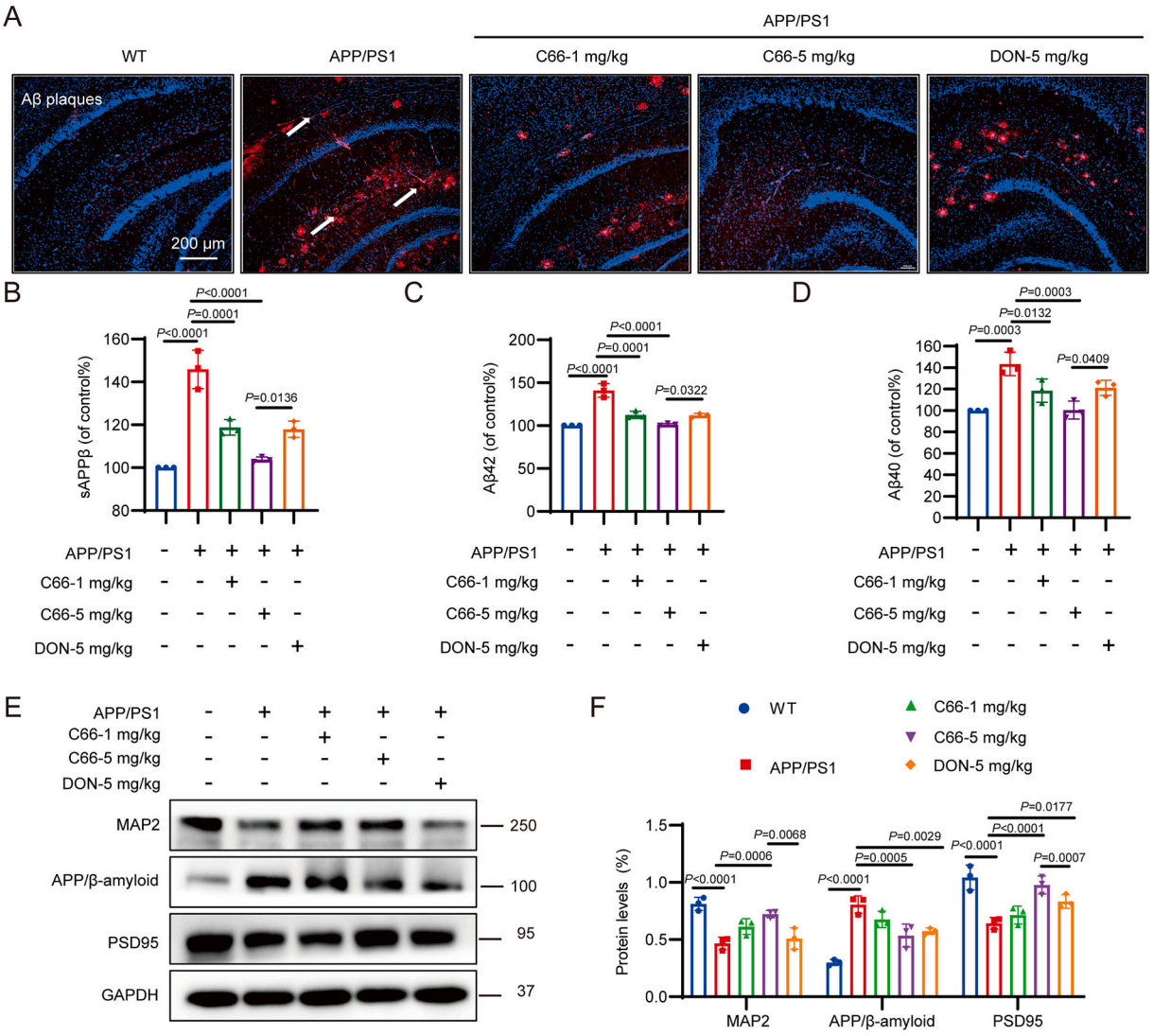

Fig. 7. C66 ameliorates AD pathology of APP/PS1 mice. (A) Representative images of Aβ plaques in the hippocampus of mouse. (B–D) Levels of sAPPβ, Aβ42, and Aβ40 in the hippocampus were measured by ELISA assays. (E–F) Expression levels of Map2, APP/β-amyloid and PSD95 were examined by western blot, and quantified with Image J software.

mice (Fig. 7E–F). Notably, the high-dose C66 group exhibited better therapeutic efficacy compared to equimolar donepezil treatment, suggesting C66's unique multimodal mechanism of action in AD pathogenesis.

3.8. C66 decreases excessive neuroinflammation in APP/PS1 mice

Neuroinflammation is an early pathological manifestation of AD, and reducing excessive inflammation could effectively prevent the development of AD. We had previously established that C66 markedly inhibited Aβ-induced inflammatory responses in BV2. In vivo, C66 treatment greatly decreased abnormal aggregation and proliferation of microglia and astrocytes in the hippocampus of APP/PS1 mice (Fig. 8A). In addition, WB results showed that C66 helped to reduce P65 nuclear translocation, and the levels of proinflammatory cytokines, TNF-α, IL-1β, and IL-18 in a dose-dependent manner. It could be seen that the anti-inflammatory effect of C66 was superior to that of donepezil (Fig. 8B–C). These results confirm that C66 effectively mitigates AD-associated neuroinflammation in vivo.

3.9. C66 reduces neuronal loss of APP/PS1 mice via inhibiting the JNK pathway

Neuronal loss is a direct cause of cognitive impairments in AD. Inhibition of neuronal apoptosis proved an effective strategy for preventing neuronal loss, thus achieving the purpose of ameliorating

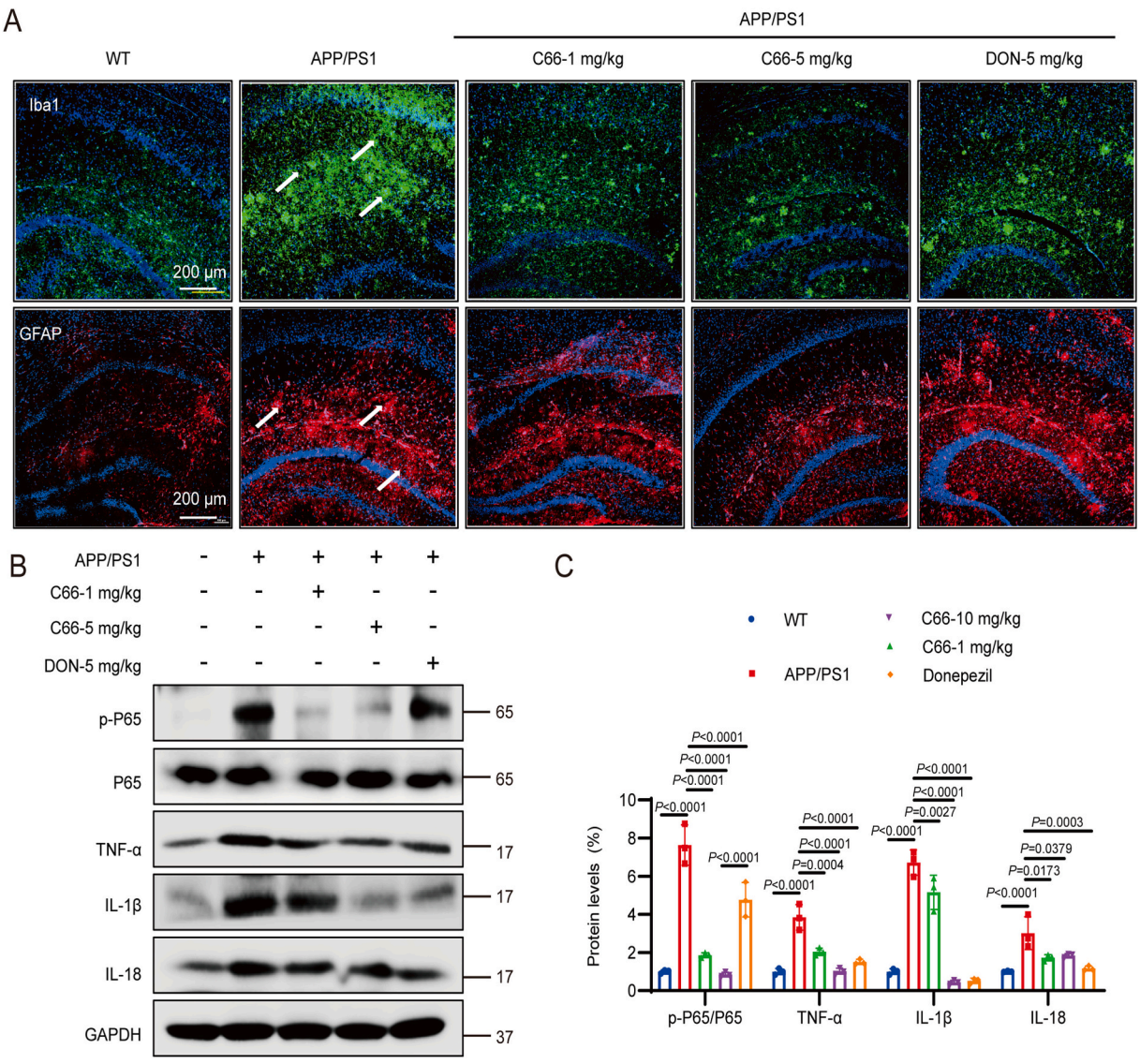

Fig. 8. C66 decreases excessive neuroinflammation in APP/PS1 mice. (A) Representative IF images of microglia (Iba1) and astrocytes (GFAP) in the hippocampus. Scale bar 200 μm. (B–C) Levels of p-P65, P65, TNF-α, IL-1β and IL-18 were detected by WB. Bands were quantified with Image J software.

cognitive function. As shown in IF images, C66 treatment reduced neuronal loss in the hippocampus of APP/PS1 mice (Fig. 9A). Afterwards, we assessed the expression levels of apoptosis-related proteins. WB results demonstrated that C66 notably elevated the ratio of Bcl-2/Bax and decreased the activation of Caspase-3 (Fig. 9B–C). Furthermore, C66 offered neuronal protection by suppressing JNK phosphorylation in tissues, consistent with in vitro experiments (Fig. 9D–E). Overall, existing outcomes demonstrated that C66 reduced neuronal apoptosis via inhibiting the JNK pathway in APP/PS1 mice.

4. Discussion

In the current study, we demonstrates that C66, a novel synthetic compound, exhibits multimodal neuroprotective effects across both cellular and animal models of AD. In vitro studies revealed that C66 pretreatment preserves mitochondrial membrane potential, reduces oxidative stress (ROS accumulation), and attenuates Aβ-induced cytotoxicity in both PC12 cells and primary cortical neurons. In APP/PS1 transgenic mice, C66 administration ameliorated key AD pathologies, including: Amyloid plaque deposition, synaptic protein loss, hippocampal neuronal degeneration, neuroinflammation, and cognitive decline. Noticeably, C66 at a dose of 5 mg/kg conferred better improved properties than the clinical comparator drug donepezil at 5 mg/kg. Mechanistic studies established that these protective effects are mediated through potent inhibition of JNK pathway activation. These findings position C66 as a promising therapeutic candidate for AD.

AD poses an escalating global health challenge, necessitating the development of cost-effective small-molecule therapeutics with favorable pharmacokinetic profiles. The natural polyphenol curcumin, derived from turmeric (*Curcuma longa*) rhizomes, has emerged as a promising lead compound due to its multimodal neuroprotective effects [24]. Extensive preclinical evidence demonstrates curcumin's ability to: mitigate oxidative stress through free radical scavenging, suppress neuroinflammatory pathways (NF-κB, JNK), and modulate amyloid/tau pathology [25,26]. Clinical observations correlate curcumin supplementation with enhanced cognitive performance in non-demented adults, concomitant with reduced amyloid deposition in memory-related brain regions [25]. Interestingly, curcumin upregulates brain-derived neurotrophic factor (BDNF), a critical neurotrophin deficient in AD and depression [27], while its ability to cross the blood-brain barrier addresses a key limitation of many neurotherapeutics.These pharmacological attributes, combined with centuries of traditional use

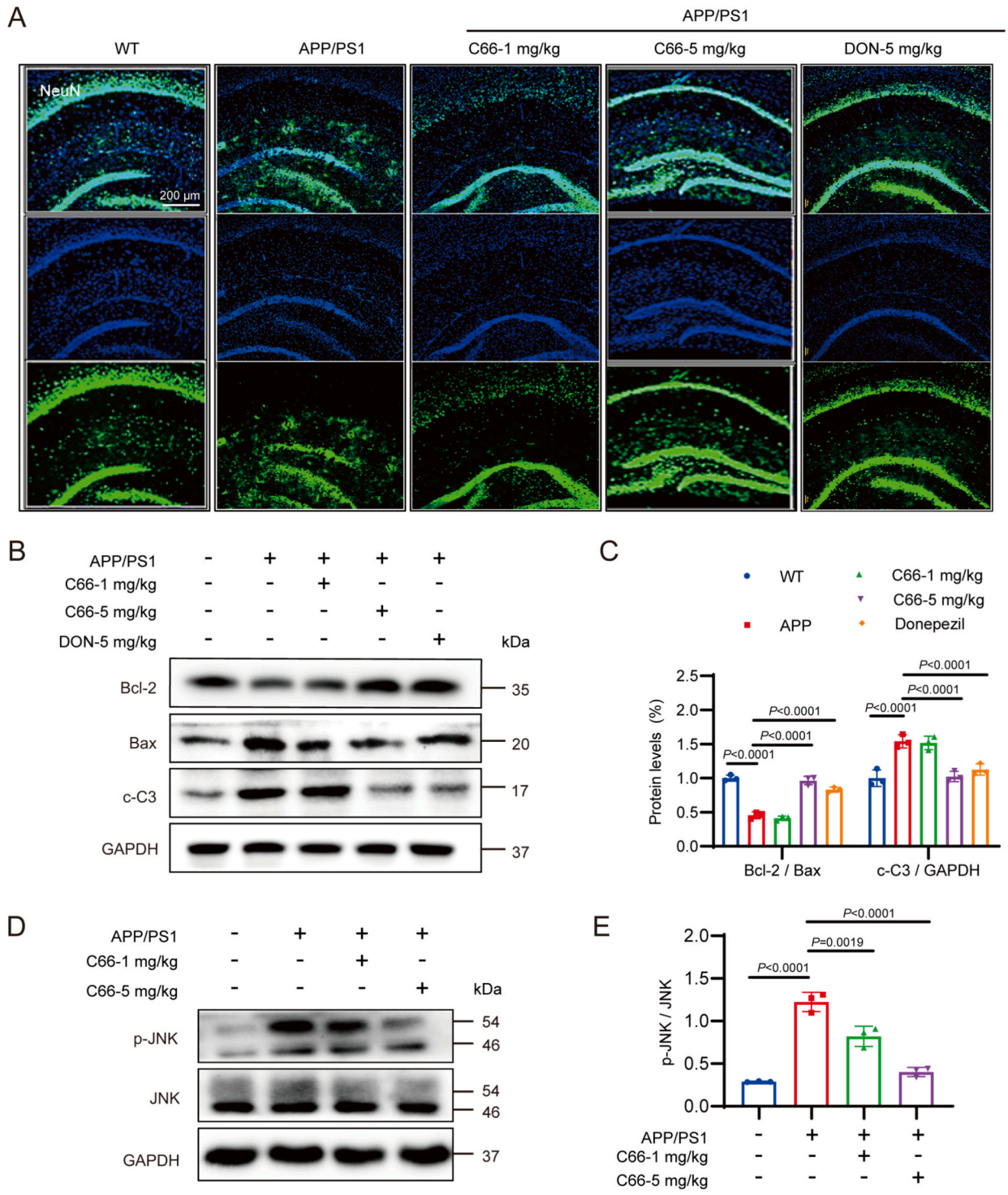

Fig. 9. C66 reduces neuronal loss of APP/PS1 mice via inhibiting the JNK pathway. (A) Representative IF images of neurons (NeuN) in the hippocampus. (B–C) Expression levels of Bcl-2, Bax, cleaved-Caspase3 were determined by western blot in the hippocampus of mice. (D–E) Expression levels of p-JNK and JNK were determined by western blot in the hippocampus of mice.

and established safety profiles, position curcumin as an ideal scaffold for developing improved AD therapeutics like its derivative C66.

C66, our laboratory-developed symmetric mono-carbonyl curcumin analog, retains the beneficial pharmacophores of curcumin while demonstrating superior drug-like properties, including enhanced chemical stability, oral bioavailability, and reduced toxicity. As previously reported, C66 exhibits potent anti-inflammatory and antioxidant activities through selective JNK pathway modulation in various disease models [9]. Our current findings reveal that C66 mediates neuroprotection through two complementary mechanisms: direct cytoprotection in neurons by maintaining mitochondrial function and reducing oxidative stress, and indirect protection via suppression of microglial activation and subsequent neurotoxic cytokine release. This dual-action pharmacodynamics likely underlies C66's superior efficacy compared to single-target drugs like donepezil. The clinical potential of C66 is underscored by its recent approval from China's National Medical

Products Administration for Phase I clinical trials in diabetic nephropathy. This regulatory milestone highlights C66's promise for treating diabetes-associated comorbidities, particularly given the well-established epidemiological link between type 2 diabetes and AD risk [28]. Pathophysiologically, diabetes may promote AD through cerebrovascular damage, chronic inflammation, and metabolic dysregulation - all processes potentially modifiable by C66's known mechanisms. Our ongoing research focuses on elucidating C66's efficacy in diabetes-associated AD models, which may establish a novel paradigm for developing multi-target therapies against AD's complex pathology.

The JNK pathway has emerged as a pivotal therapeutic target in AD, orchestrating multiple pathological processes including neuroinflammation, apoptosis, and amyloidogenesis. For example, timosaponin B-II attenuates LPS-induced neuroinflammation via JNK suppression in BV2 cells [29]; VB-037 reduces Aβ aggregation and neuronal death through JNK inhibition [30]; Nicotinamide mononucleotide exerts neuroprotection by blocking JNK activation [31]. Our results demonstrate that C66 mediates its therapeutic effects primarily through dose-dependent JNK phosphorylation inhibition, as validated using the specific JNK inhibitor SP600125. Notably, C66 exhibits cell-type specific potency, achieving significant anti-inflammatory effects in BV2 microglia at 5 μM, while requiring 10 μM for robust neuroprotection in PC12 cells - likely reflecting differential cellular uptake or JNK isoform expression. It is worth mentioning that the positive control, donepezil, functions as an acetylcholinesterase inhibitor and operates through a different mechanism than C66. The current study seems to imply that we are supposed to seek new targets in order to achieve enhanced therapeutic effects for AD, and JNK appears to be a promising target to consider. Even though our laboratory had previously verified the direct binding and inhibitory effects of C66 on the JNK protein, we acknowledge that C66 may have additional potential targets of action, which are also implicated in its pharmacological effects [8]. Except for P65 and Bcl-2/Bax, JNK inhibition by C66 may affect other signaling pathways, including PI3K/AKT, to exert its neuroprotective effects. These findings significantly advance our understanding of JNK's central role in AD pathogenesis while underscoring the need for further investigation into C66's complete mechanism of action and potential synergistic pathways.

Collectively, our results establish that C66, a synthetic curcumin derivative, exerts multimodal therapeutic effects in AD models through selective inhibition of the JNK signaling pathway. Notably, C66 showed superior efficacy to the clinical standard donepezil, while maintaining an excellent safety profile. These findings position C66 as a promising next-generation therapeutic candidate that addresses multiple pathological hallmarks of AD through a unified molecular mechanism.

Authors' contributions

Houming Yu, Jurui Wei and Xia Zhao contributed to the literature search and study design. Xiong Li participated in the drafting of the article. Guang Liang and Xia Zhao contributed to the manuscript modification. Li Xiong, Qin Yu, Linjie Chen,Yu Deng, Qi Ai, Xiaoxia Xu, Ziyao Meng carried out the experiments. Fan Chen contribute to the methodology. All authors read and approved the final manuscript.

CRediT authorship contribution statement

Li Xiong: Writing – original draft, Data curation. **Qin Yu:** Data curation. **Linjie Chen:** Data curation. **Yu Deng:** Data curation. **Qi Ai:** Data curation. **Xiaoxia Xu:** Formal analysis. **Ziyao Meng:** Formal analysis. **Fan Chen:** Methodology, Funding acquisition. **Xia Zhao:** Writing – review & editing, Project administration, Funding acquisition, Conceptualization. **Jurui Wei:** Resources, Project administration, Conceptualization. **Houming Yu:** Validation, Project administration, Methodology, Conceptualization.

Ethics approval and consent to participate

All experiments and procedures were performed in accordance with the Hangzhou Medical College Animal Care Guidelines and approved by the Ethics Committee of the School of Pharmacy, Hangzhou Medical College (No. 2023-052).

Author statement

All authors have read and approved the final manuscript. All authors contributed to data analysis, drafting or revising the article, agreed on the journal to which the article will be submitted, gave final approval of the version to be published, and agreed to be accountable for all aspects of the work.

Funding

This study was supported by Natural Science Foundation of Zhejiang Province (LQ23H090018 to X.Z.), Hangzhou Natural Science Foundation (2024SZRYBH090002 to X.Z.), Medical and Health Science and Technology Project of Zhejiang Province (2025KY1032 to X.Z.) and Basic Scientific Research Funds of Department of Education of Zhejiang Province (KYYB202010 to F.C.). We would like to thank the support from the Scientific Research Center, Hangzhou Medical College.

Declaration of competing interest

The authors declare that they have no known competing financial interests or personal relationships that could have appeared to influence the work reported in this paper.

Acknowledgements

This study was supported by Natural Science Foundation of Zhejiang province (LQ23H090018 to X.Z.), Hangzhou Natural Science Foundation (2024SZRYBH090002 to X.Z.), Medical and Health Science and Technology Project of Zhejiang Province (2025KY1032 to X.Z.) and Basic Scientific Research Funds of Department of Education of Zhejiang Province (KYYB202010 to F.C.). We would like to thank the support from the Scientific Research Center, Hangzhou Medical College. We would like to thank Hangzhou Medical College for providing the experimental facility to support this research.

Data availability

Data will be made available on request.

References

[1] A.A. Rostagno, Pathogenesis of Alzheimer's disease, Int. J. Mol. Sci. 24 (1) (2022).
[2] W. Liu, S. Gauthier, J. Jia, Alzheimer's disease: current status and perspective, Sci. Bull. (Beijing) 67 (24) (2022) 2494–2497.
[3] Y. Yan, et al., Osthole promotes endogenous neural stem cell proliferation and improved neurological function through notch signaling pathway in mice acute mechanical brain injury, Brain Behav. Immun. 67 (2018) 118–129.
[4] W. Sun, J. Zhao, C. Li, Dexmedetomidine provides protection against hippocampal neuron apoptosis and cognitive impairment in mice with Alzheimer's disease by mediating the miR-129/YAP1/JAG1 Axis, Mol. Neurobiol. 57 (12) (2020) 5044–5055.
[5] Y. Liu, et al., Electroacupuncture inhibits hippocampal neuronal apoptosis and improves cognitive dysfunction in mice with vascular dementia via the JNK signaling pathway, Acupunct. Med. 41 (5) (2023) 284–296.
[6] S.J. Shin, et al., Red ginseng attenuates aβ-induced mitochondrial dysfunction and aβ-mediated pathology in an animal model of Alzheimer's disease, Int. J. Mol. Sci. 20 (12) (2019).
[7] C.G. Weindel, et al., Mitochondrial ROS promotes susceptibility to infection via gasdermin D-mediated necroptosis, Cell 185 (17) (2022) 3214–3231.e23.
[8] Y. Pan, et al., Inhibition of JNK phosphorylation by a novel curcumin analog prevents high glucose-induced inflammation and apoptosis in cardiomyocytes and the development of diabetic cardiomyopathy, Diabetes 63 (10) (2014) 3497–3511.

[9] L. Ye, et al., Curcumin analogue C66 attenuates obesity-induced renal injury by inhibiting chronic inflammation, Biomed. Pharmacother. 137 (2021) 111418.
[10] M. Salazar, et al., COVID-19 and its relationship with hypertension and cardiovascular disease, Hipertens. Riesgo Vasc. 37 (4) (2020) 176–180.
[11] E.K. Kim, E.J. Choi, Pathological roles of MAPK signaling pathways in human diseases, Biochim. Biophys. Acta 1802 (4) (2010) 396–405.
[12] S.C. Hepp Rehfeldt, et al., C-Jun N-terminal kinase inhibitors as potential leads for new therapeutics for Alzheimer's diseases, Int. J. Mol. Sci. 21 (24) (2020).
[13] J. Yue, J.M. López, Understanding MAPK signaling pathways in apoptosis, Int. J. Mol. Sci. 21 (7) (2020).
[14] B. Cai, et al., A synthetic diosgenin primary amine derivative attenuates LPS-stimulated inflammation via inhibition of NF-κB and JNK MAPK signaling in microglial BV2 cells, Int. Immunopharmacol. 61 (2018) 204–214.
[15] H. Chen, et al., Curcumin derivative C66 suppresses pancreatic Cancer progression through the inhibition of JNK-mediated inflammation, Molecules (10) (2022) 27.
[16] E. Ferrari, et al., From cell lines to pluripotent stem cells for modelling Parkinson's disease, J. Neurosci. Methods 340 (2020) 108741.
[17] K. Ono, T. Watanabe-Nakayama, Aggregation and structure of amyloid β-protein, Neurochem. Int. 151 (2021) 105208.
[18] A.B. Reiss, et al., Amyloid toxicity in Alzheimer's disease, Rev. Neurosci. 29 (6) (2018) 613–627.
[19] X. Zhao, et al., Artemisinin attenuates amyloid-induced brain inflammation and memory impairments by modulating TLR4/NF-κB signaling, Int. J. Mol. Sci. 23 (11) (2022).
[20] L. She, et al., Ginsenoside Rk3 ameliorates aβ-induced neurotoxicity in APP/PS1 model mice via AMPK signaling pathway, Biomed. Pharmacother. 158 (2023) 114192.
[21] X. Zhao, et al., B-Amyloid binds to microglia Dectin-1 to induce inflammatory response in the pathogenesis of Alzheimer's disease, Int. J. Biol. Sci. 19 (10) (2023) 3249–3265.
[22] S.H. Nies, et al., Spreading of Alzheimer tau seeds is enhanced by aging and template matching with limited impact of amyloid-β, J. Biol. Chem. 297 (4) (2021) 101159.
[23] Z. Xie, et al., The Dual Nature of Microglia in Alzheimer's Disease: A Microglia-Neuron Crosstalk Perspective, Neuroscientist 29 (5) (2023) 616–638.
[24] A.B. Kunnumakkara, et al., Curcumin, the golden nutraceutical: multitargeting for multiple chronic diseases, Br. J. Pharmacol. 174 (11) (2017) 1325–1348.
[25] B. Chen, et al., Curcumin alleviates oxidative stress, Neuroinflammation, and promotes behavioral recovery after traumatic brain injury, Curr. Neurovasc. Res. 20 (1) (2023) 43–53.
[26] G.W. Small, et al., Memory and brain amyloid and tau effects of a bioavailable form of curcumin in non-demented adults: a double-blind, placebo-controlled 18-month trial, Am. J. Geriatr. Psychiatry 26 (3) (2018) 266–277.
[27] P. Sarraf, et al., Short-term curcumin supplementation enhances serum brain-derived neurotrophic factor in adult men and women: a systematic review and dose-response meta-analysis of randomized controlled trials, Nutr. Res. 69 (2019) 1–8.
[28] J. Graff-Radford, et al., New insights into atypical Alzheimer's disease in the era of biomarkers, Lancet Neurol. 20 (3) (2021) 222–234.
[29] W.Q. Lu, et al., Timosaponin B-II inhibits pro-inflammatory cytokine induction by lipopolysaccharide in BV2 cells, Arch. Pharm. Res. 32 (9) (2009) 1301–1308.
[30] Y.J. Chiu, et al., Novel compound VB-037 inhibits aβ aggregation and promotes neurite outgrowth through enhancement of HSP27 and reduction of P38 and JNK-mediated inflammation in cell models for Alzheimer's disease, Neurochem. Int. 125 (2019) 175–186.
[31] Z. Yao, et al., Nicotinamide mononucleotide inhibits JNK activation to reverse Alzheimer disease, Neurosci. Lett. 647 (2017) 133–140.